Chinese Chemical Letters 34 (2023) 107666

Contents lists available at ScienceDirect

Chinese Chemical Letters

journal homepage: www.elsevier.com/locate/cclet

Iridium photosensitizer constructed liposomes with hypoxia-activated prodrug to destrust hepatocellular carcinoma

Shuangling Luo, Chao Liang, Qianling Zhang, Pingyu Zhang*

College of Chemistry and Environmental Engineering, Shenzhen University, Shenzhen 518060, China

ARTICLE INFO

Article history:
Received 16 April 2022
Revised 1 July 2022
Accepted 7 July 2022
Available online 9 July 2022

Keywords:
Hypoxia activation
Iridium photosensitizer
Ferroptosis
Photodynamic therapy
Chemotherapy

ABSTRACT

Hypoxic tumor microenvironment is a major challenge for photodynamic therapy (PDT). To overcome this problem, PDT combined hypoxia-activated chemotherapy is a promising strategy for hypoxic cancer therapy. Herein, a multifunctional liposome (AQ4N-**Ir1**-sorafenib-liposome) is prepared by encapsulating a hypoxia-activated prodrug AQ4N, a photosensitizer iridium(III) complex and hepatocellular carcinoma (HCC) targeting drug sorafenib, for synergistic therapy of HCC. **Ir1**-mediated PDT upon irradiation induces ROS generation and hypoxic environment, which leads to the disassembly of the liposome and activates the antitumor activity of AQ4N. Meantime, the co-delivered sorafenib could effectively target therapy of HCC. It is noted that ferroptosis mechanism is proved during the treatment. This work contributes to the design of hypoxia-responsive multifunctional liposome for combination of chemotherapy, targeting therapy and PDT. It is a promising strategy for hypoxic HCC therapy.

As is known to all, hepatocellular carcinoma (HCC) originates from liver cells and is a malignant tumor with high mortality [1–3]. HCC is highly secretive and usually asymptomatic in the early stage, but most patients of HCC are diagnosed in an advanced stage. Sorafenib, a chemotherapeutic drug, has been approved by the FDA (USA Food and Drug Administration) and EMEA (European Medicines Evaluation Agency) for the treatment of advanced liver cancer [4]. It has been shown to be effective in enhancing survival time in patients, but its efficacy is still not satisfactory due to its poor solubility, low bioavailability and long term drug resistance [5–7]. Therefore, there is an urgent need to search for new treatments for HCC.

Photodynamic therapy (PDT) is a method in which a photosensitizer at the tumor site is activated by a specific wavelength of light and reacts with surrounding O_2 molecules to produce a large amount of $^1O_2$, which strikes the intracellular redox balance and consequently kills the tumor cells [8–10]. However, compared with normal tissues, solid tumors have uneven growth, malfunctioning vascular system, and insufficient blood flow, resulting in hypoxia microenvironment [11–13], thus the therapeutic effect of PDT will be greatly reduced. In addition, such O_2-dependent PDT, due to oxygen consumption and the antivascular effect of tumor microenvironment, tending to exacerbate tumor hypoxia, mediating tumor resistance to chemotherapy [14], and increasing the risk of tumor metastasis and recurrence [15,16]. In order to improve the antitumor activity of PDT, it has been reported to relieving tumor hypoxia various strategies, such as the use of hemoglobin (Hb) molecules [17,18], full load of the perfluorocarbon oxygen to carry O_2 to the tumor site [19], or enzyme catalysis *in situ* generation of O_2 [20–22], also using the respiratory inhibitors (metformin) inhibiting tumor O_2 consumption [23]. Although these strategies enhance therapeutic efficacy to some extent, they may be limited by tumor heterogeneity and lack of accuracy at hypoxic sites [15,24]. In contrast to the strategies to alleviate tumor hypoxia, more effective and more selective cancer therapy using tumor hypoxia has received widespread attention, such as some hypoxia activated prodrugs (TPZ, AQ4N, TH-302), which are already in clinical trials [25–30]. They can be reduced from nontoxic prodrugs to toxic drugs under hypoxic condition. The combination of PDT and hypoxia activated prodrugs can effectively achieve cascade therapy to overcome the hypoxic problem of the tumor and achieve complementary enhancement. In addition, chemotherapy can further eliminate the residual cancer cells due to uneven tumor regions and unobserved margins, and inhibit tumor recurrence [31,32]. Therefore, the preparation of a multifunctional therapeutic system for photodynamic/hypoxic activation/chemotherapy combination therapy can overcome the defects of each single treatment method, and is a promising innovative strategy to achieve great therapeutic effect. The nanotechnology-based drug delivery system provides a good platform for realizing these strategies, which can not only improve the treatment efficiency of chemotherapy drugs and re-

* Corresponding author.
E-mail address: p.zhang6@szu.edu.cn (P. Zhang).

https://doi.org/10.1016/j.cclet.2022.07.009
1001-8417/

duce the toxicity of the system [33], but also realize multi-pathway treatment [34].

One of the strategic designs for efficient photosensitizers can be rationalized by improvement in the triplet excited state population for the generation of ROS through the introduction of heavy atoms as a result of the heavy-atom effect, such as Br, I or transition metals into the chromophores [35–37]. In recent years, luminescent transition metal complexes with suitable excited states have been known to be promising photo-theranostic candidates owing to their superior photochemical and photophysical properties [38–44]. Among various metal complexes, Ir(III) complexes are widely employed as photosensitizers due to their high photostability, cellular uptake, impressive singlet oxygen ($^1O_2$) generation quantum yield and unique photo-antitumor properties [45–52]. However, most of the Ir(III) complexes are hydrophobic and their photochemotherapeutic effects in the hydrophilic environment of cellular systems are greatly reduced [53]. Thus, developing a novel Ir(III)-based anticancer system with appropriate water solubility, good biosafety, and excellent $^1O_2$ generation ability and thereafter extend its application in PDT is highly challenging.

In recent years, ferroptosis, an iron-dependent modality of cancer cell death, has received increasing attention [54]. It is driven by some inducers that can directly or indirectly down-regulates glutathione peroxidase 4 (GPX4) activity, resulting in intracellular lipid hydroperoxides (LPO) metabolism disorder, thereby damaging cell structure and integrity [55,56]. Inhibition of GPX4 activity by down-regulation of GSH level is a typical ferroptosis event [57]. This pathway avoids the MDR effect associated with membrane proteins and has inherently potent in eliminating resistant tumor cells [58–60]. Therefore, introducing ferroptosis into antitumor therapy might be a very promising treatment approach.

Herein, we develop a AQ4N-**Ir1**-sorafenib liposome encapsulated three functional parts: 1) a hypoxia activated prodrug-AQ4N; 2) a photosensitizer iridium(III) complex-**Ir1**; 3) a HCC targeting therapy drug-sorafenib. Upon light irradiation, **Ir1** generates ROS, which lead to the damage of the liposome, thus the co-delivered sorafenib was released. Furthermore, **Ir1**-mediated PDT inducing hypoxic environment activates AQ4N for improved hypoxic cancer cell-killing. The liposome could induce HCC ferroptosis and effectively target therapy of HCC (Scheme 1). This PDT-induced and hypoxia-activated synergistic targeting therapy is a promising strategy for HCC therapy in future.

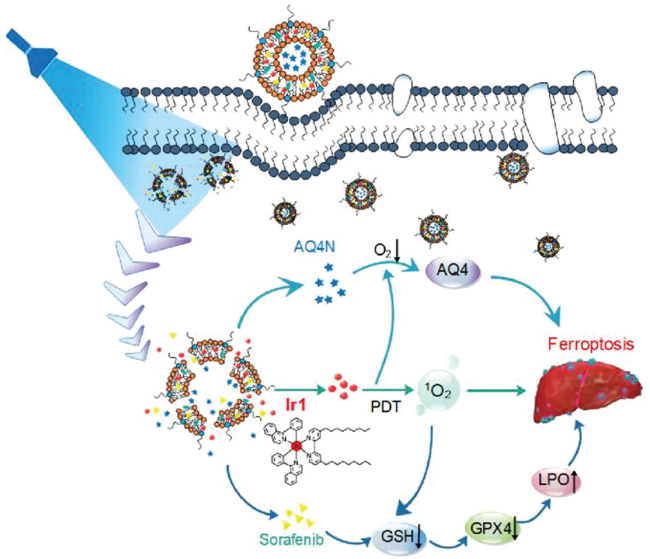

Scheme 1. The mechanism scheme of the AQ4N-**Ir1**-sorafenib-liposome for hepatocellular carcinoma therapy.

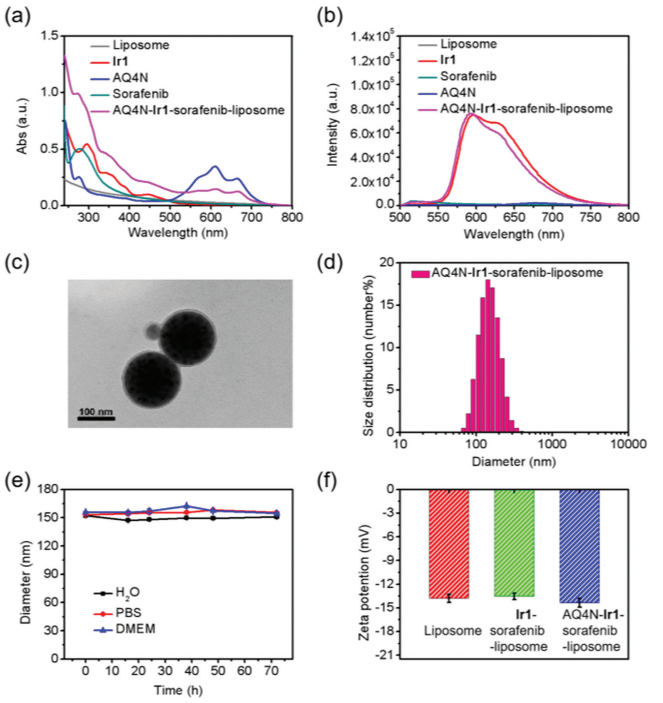

Fig. 1. Characterization of AQ4N-**Ir1**-sorafenib-liposome. (a) The UV–vis absorbance spectra of the free liposome, **Ir1**, sorafenib, AQ4N and AQ4N-**Ir1**-sorafenib-liposome. (b) The fluorescence spectra of the free liposome, **Ir1**, sorafenib, AQ4N and AQ4N-**Ir1**-sorafenib-liposome. (c) The TEM image of AQ4N-**Ir1**-sorafenib-liposome. (d) DLS size distribution of AQ4N-**Ir1**-sorafenib-liposome. (e) Hydrodynamic diameters of AQ4N-**Ir1**-sorafenib-liposome in H_2O, PBS and DMEM for 72 h, respectively. (f) The zeta potential of the free liposome, **Ir1**-sorafenib-liposome and AQ4N-**Ir1**-sorafenib-liposome.

A hydrophobic iridium(III) complex (**Ir1**) was firstly designed and synthesized. **Ir1** was fully characterized by ^1H NMR, ^{13}C NMR and ESI-MS spectra in the experimental section and Figs. S1-S3 (Supporting information). Then a high biocompatible liposome was prepared as reported method [20,28]. Sorafenib and **Ir1** were wrap into the hydrophobic layer of the liposome, while AQ4N was in the hydrophilic layer (Scheme S1 in Supporting information). As shown in Fig. S4 (Supporting information), when DPPC (17.6 mg), cholesterol (6.17 mg), DSPE-mPEG5k (10 mg), sorafenib (0.9 mg) and **Ir1** (0.9 mg) at a molar ratio of 24:16:2:2:0.9, the prepared liposome was homogeneous and had a good stability, thus this ratio was used in our experiment. Then 10 mg/mL AQ4N was added to prepare AQ4N-**Ir1**-sorafenib-liposome [61]. The unencapsulated AQ4N, **Ir1** and sorafenib were removed *via* column chromatography method with a sephadex G-100 column (Fig. S5 in Supporting information). Finally, according to the absorption values of AQ4N and sorafenib at 610 nm and 265 nm, respectively, the loading efficiencies of AQ4N and sorafenib were quantitatively calculated as 10.2% and 54.7%, respectively. The loading efficiency of **Ir1** was 43% by ICP-MS measurement.

The successful encapsulation of AQ4N, **Ir1** and sorafenib into the liposome was firstly confirmed by UV–vis absorption spectra. The characteristic absorbance peaks obviously changed after encapsulation of each drug (Fig. 1a and Fig. S6 in Supporting information). Next the fluorescence spectra suggested that physically encapsulation by liposome cannot change the emission performance of **Ir1** (Fig. 1b). The obtained AQ4N-**Ir1**-sorafenib-liposome showed uniform sphere-like morphology by transmittance electron microscopy (TEM) (Fig. 1c). As measured by dynamic light scattering (DLS), the as-prepared AQ4N-**Ir1**-sorafenib-liposome showed

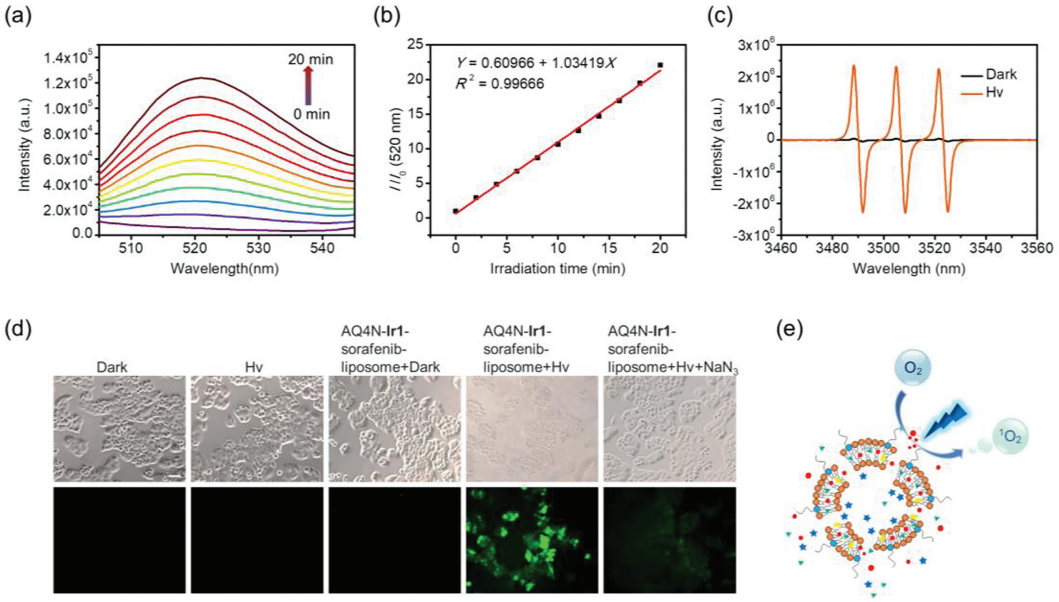

Fig. 2. (a) The fluorescence intensity of DCFH-DA (10 μmol/L) and AQ4N-**Ir1**-sorafenib-liposome (10 μmol/L based on **Ir1**) under light irradiation (0–20 min, 2 min for each line). (b) The relative fluorescence intensity at 520 nm in (a). (c) ESR spectra of TEMP and AQ4N-**Ir1**-sorafenib-liposome mixing solution before and after light irradiation (465 nm, 6.5 mW/cm^2). (d) The fluorescence images of Hep-G2 cells stained with DCFH-DA (10 μmol/L) after various treatments. DCFH-DA: λ_{ex}= 460 nm, λ_{em}= 510–550 nm. Scale bar: 50 μm. (e) The schematic diagram of AQ4N-**Ir1**-sorafenib-liposome producing ROS under light irradiation.

a size distribution with a mean diameter of ~150 nm (Fig. 1d), and maintained a good stability in the H_2O/PBS/DMEM medium for 72 h (Fig. 1e). The zeta potential of the AQ4N-**Ir1**-sorafenib-liposome was presented a negative charge at about −14.4 mV, which was similar to a free liposome (−13.8 mV) (Fig. 1f). Although **Ir1** is positive charge, it is in the hydrophobic layer and thus has a very small impact on zeta potential.

Next, we measured ROS generation in solution using DCFH-DA (2,7-dichlorofluorescein diacetate), which could react with ROS to cause an increase in the fluorescence. As shown in Figs. 2a and b, the enhancement of the fluorescence exhibited that the AQ4N-**Ir1**-sorafenib-liposome could generate ROS under light irradiation (465 nm, 6.5 mW/cm^2), and calculated a linear relationship of I/I_0 at 520 nm depending on the irradiation time. We further adopted electron spin resonance (ESR) to detect $^1O_2$ generation. The 2,2,6,6-tetramethylpiperidine (TEMP) was used to trap $^1O_2$. As shown in Fig. 2c, a strong three-line signal shown between 3480 and 3530 G in AQ4N-**Ir1**-sorafenib-liposome and TEMP solution was observed under light irradiation. By contrast, there was no signal observed under dark. Other ROS, such as $^{\bullet}$OH, was also measured using methylene blue (MB) upon light irradiation. As shown in Fig. S7 (Supporting information), the absorption peak of MB did not change under light irradiation. The above results showed that AQ4N-**Ir1**-sorafenib-liposome produced $^1O_2$ but not $^{\bullet}$OH after light irradiation. As far as we know, the only component in the liposome that can produce ROS was **Ir1**. We also found ROS generation in the free **Ir1** solution (Fig. S8 in Supporting information). We further studied intracellular ROS generation based on AQ4N-**Ir1**-sorafenib-liposome for PDT. As shown in Fig. 2d, the results showed that significant green fluorescence of DCF was observed in the AQ4N-**Ir1**-sorafenib-liposome+Hv group, indicating the production of ROS. While the fluorescence signal was weakened after NaN_3 was added, which proved that the ROS mainly observed in cells was $^1O_2$. These results demonstrated that AQ4N-**Ir1**-sorafenib-liposome possessed superior $^1O_2$ generation capability under light irradiation (Fig. 2e).

The cell viabilities of AQ4N-**Ir1**-sorafenib-liposome towards Hep-G2 cells were investigated by a standard MTT assay. Under normoxia (Fig. 3a and Table 1), AQ4N-**Ir1**-sorafenib-liposome and sorafenib showed slight dark-cytotoxicity towards Hep-G2 cells after 24 h drug exposure compared to **Ir1** and AQ4N. After 465 nm light irradiation, AQ4N-**Ir1**-sorafenib exhibited photo-cytotoxicity, the $IC_{50,\ Light}$ value was 0.39 μmol/L (based on the concentration of **Ir1**) in the normoxia, which was much lower than **Ir1** under irradiation. This is maybe due to the additional toxicity of sorafenib in the AQ4N-**Ir1**-sorafenib-liposome compared to the free **Ir1**. In addition, 5-aminolevulinic acid (5-ALA) was used as a positive control. Low dark- and photo-toxicities (both $IC_{50,\ dark}$ and $IC_{50,\ light}$ > 10 μmol/L) were showed in Hep-G2 cells. Considering that AQ4N is a hypoxic activator, it can be reduced to high toxic AQ4 [62,63]. We further studied the cytotoxicity of the liposome under hypoxia (1% O_2) (Fig. 3b). Compared with normoxia, AQ4N was highly toxic under hypoxia, and AQ4N-**Ir1**-sorafenib-liposome has similar toxic effects in the dark or under irradiation in hypoxia. The $IC_{50,\ Light}$ and $IC_{50,\ Dark}$ values of AQ4N-**Ir1**-sorafenib-liposome were all 0.06 μmol/L in the hypoxia (Table 1), which was much lower than that under normoxia, meaning that AQ4N plays an important role under hypoxia. The **Ir1**+Hv group in hypoxia also showed slightly phototoxicity, which may be because **Ir1** can photo-oxidize NADH (Fig. S9 in Supporting information) in hypoxia, which is the similar result as reported [48].

In addition, calcein acetoxymethyl ester (Calcein-AM) and propidium iodide (PI) co-staining were further studied to observe live and dead cells, respectively (Fig. S10 in Supporting information). Calcein-AM could stain the living cells in green, while PI could stain the dead cells in red. The results were consistent with the cytotoxicity. AQ4N-**Ir1**-sorafenib-liposome can kill cancer cells both in the normoxia and hypoxia. We further studied the biosafety of AQ4N-**Ir1**-sorafenib liposomes in zebrafish with green fluorescent protein (GFP) as a universal biomarker (Fig. S11 in Supporting information). After 4 days of treatment with AQ4N-**Ir1**-sorafenib-liposome, zebrafish still survived without obvious vascular damage, demonstrating a good biosafety.

As we know, $^1O_2$ can oxidize GSH to GSSG and destroy the redox balance in cancer cells [58]. We studied this property in solution using 5,5′-dithiobis(2-nitrobenzoic acid) (DTNB) as an indica-

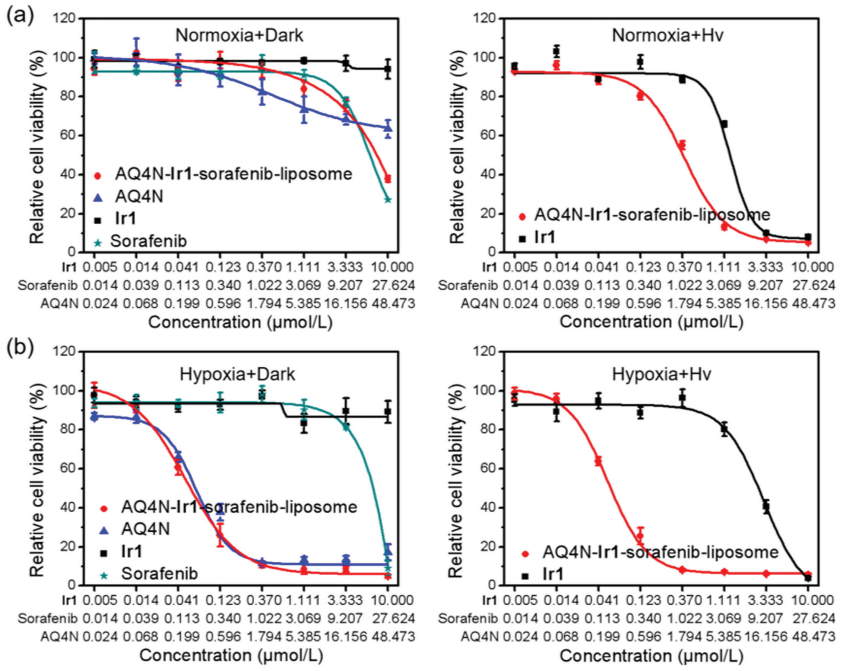

Fig. 3. Cytotoxicity of AQ4N-**Ir1**-sorafenib-liposome, **Ir1**, sorafenib and AQ4N towards Hep-G2 cells with irradiation (465 nm, 6.5 mW/cm^2) or without irradiation measured in (a) normoxia (20% O_2) and (b) hypoxia (1% O_2). The error bars were based on triplicate measurements.

Table 1
IC_{50} values (μmol/L) of the drugs towards Hep-G2 cells.[a]

Drugs	Hep-G2 cells			
	Normoxia (20% O_2) [b]		Hypoxia (1% O_2) [c]	
	$IC_{50,\ Dark}$	$IC_{50,\ Light}$	$IC_{50,\ Dark}$	$IC_{50,\ Light}$
AQ4N-**Ir1**-sorafenib-liposome	7.44 ± 0.03	0.39 ± 0.001	0.06 ± 0.001	0.06 ± 0.001
Ir1	>10	1.39 ± 0.006	>10	2.71 ± 0.009
AQ4N	>48.473	N.D.	0.34 ± 0.002	N.D.
Sorafenib	19.51 ± 0.06	N.D.	19.65 ± 0.04	N.D.
5-ALA	>10	>10	–	–

N.D. = not determined.
[a] The IC_{50} values of AQ4N-**Ir1**-sorafenib-liposome were based on the concentration of **Ir1**.
[b] Cells were cultivated under normoxia and 24 h drug exposure, washed with PBS for three times, the dark group was incubated for another 48 h in the dark, the light group followed by light irradiation (465 nm, 6.5 mW/cm^2) for 1 h and incubated in the normoxia for another 47 h.
[c] Cells were cultivated under hypoxia and 24 h drug exposure, washed with PBS for three times, the dark group was incubated for another 48 h in the dark, the light group followed by light irradiation (465 nm, 6.5 mW/cm^2) for 1 h and incubated in the hypoxia for another 47 h.

tor. As shown in Figs. 4a and b, as the irradiation time increased, the absorption peak decreased gradually at 412 nm, and the color of the solution was shallower and shallower, meaning that GSH was oxidized to GSSG. We further investigated GSH levels in Hep-G2 cells after different treatments using monobromobimane [64–66], a fluorescent probe that reacted with sulfhydryl group of GSH (Fig. 4c). The results showed that the fluorescence intensity of cells was significantly reduced after incubation with AQ4N-**Ir1**-sorafenib-liposome, and this phenomenon was more obvious in the AQ4N-**Ir1**-sorafenib-liposome+Hv group, indicating that GSH was consumed.

In cancer cells, down-regulated GSH level directly induces the inactivation of the GPX4, which damages the cellular antioxidant defense mechanism and directly or indirectly induces ferroptosis [59]. The expression of GPX4 in Hep-G2 cells was detected by Western blot assay (Fig. 4d and Fig. S12 in Supporting information). The expression of GPX4 in Dark, Hv and AQ4N groups were not affected, and the expression of GPX4 in **Ir1**+Dark group was slightly down-regulated and negligible, but the expression of GPX4 in sorafenib, **Ir1**+Hv, AQ4N-**Ir1**-sorafenib-liposome+Dark group and AQ4N-**Ir1**-sorafenib-liposome+Hv group were significantly down-regulated. It was noted that the GPX4 expression in AQ4N-**Ir1**-sorafenib-liposome+Hv group showed the greatest decrease, indicating that $^1O_2$ produced by PDT and sorafenib simultaneously induced ferroptosis.

Intracellular lipid peroxides are considered to be important biomarkers of ferroptosis [67]. The consumption of GSH inhibits the expression of GPX4, which leads to the accumulation of lipid peroxides (LPO) in cells and induces ferroptosis. A lipid peroxidation sensor, C11-BODIPY$^{581/591}$ [59,68,69], was used to detect the LPO by confocal laser scanning microscopy (CLSM) (Fig. 4e). The images of AQ4N-**Ir1**-sorafenib-liposome + Hv group showed a strong green fluorescence intensity, indicating LPO accumulation. When the group was pre-treated with DFO (deferoxamine, a ferroptosis inhibitor), and the fluorescence was weakened. However, there was very weak green fluorescence in the other groups (Fig. 4e), further confirming that AQ4N-**Ir1**-sorafenib-liposome induced the accumulation of LPO and then ferroptosis under light irradiation (Fig. 4f).

In summary, this work investigated a novel AQ4N-**Ir1**-sorafenib-liposome to achieve targeting chemotherapy, photodynamic therapy and treatment of hypoxic tumors. By utilizing the ROS gen-

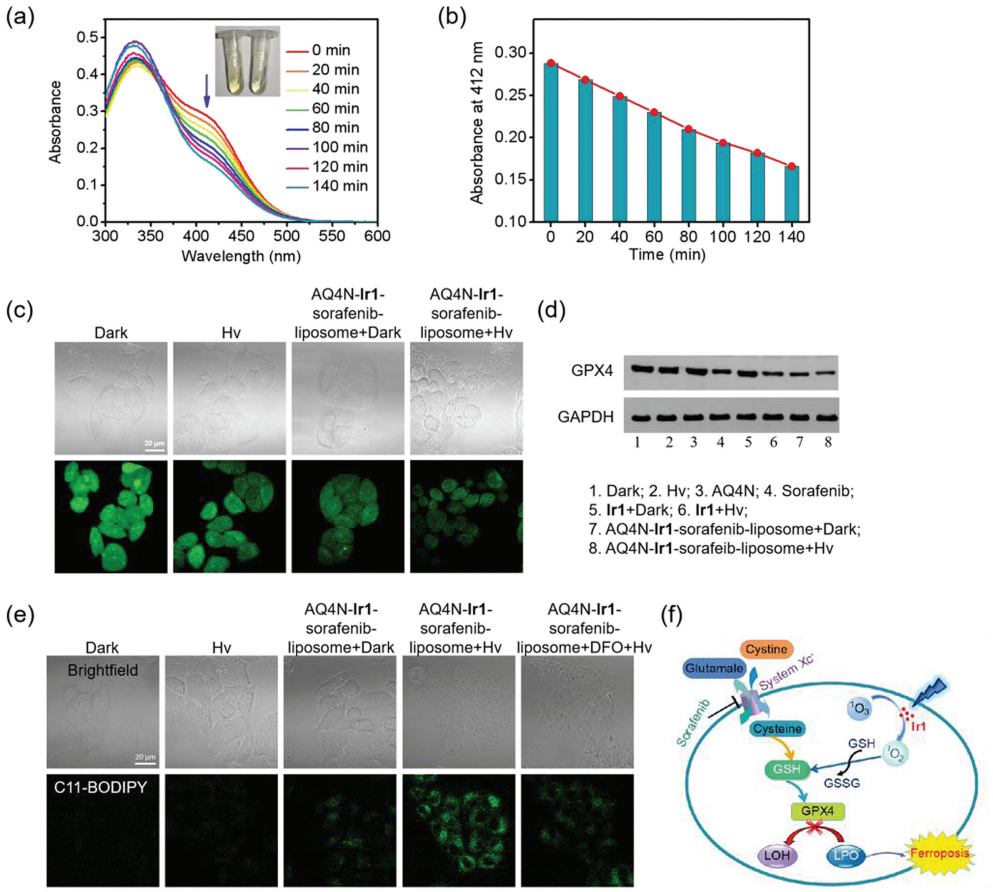

Fig. 4. (a) Time-dependent GSH consumption with AQ4N-**Ir1**-sorafenib-liposome (10 μmol/L base on **Ir1**) under irradiation (465 nm, 6.5 mW/cm^2). Inset: Images of GSH reaction solution before and after irradiation. (b) Absorption at 412 nm with irradiation time increases in (a). (c) CLSM images of cellular GSH levels detected by monobromobimane (5 μmol/L), scale bar = 20 μm. (d) Western blot analysis of GPX4 expression in Hep-G2 cells. (e) CLSM images of C11-BODIPY$^{581/591}$ stained Hep-G2 cells after various treatments, scale bar = 20 μm. The concentrations of AQ4N-**Ir1**-sorafenib-liposome, DFO and C11-BODIPY$^{581/591}$ were 2 μmol/L, 100 μmol/L and 10 μmol/L, respectively. Light irradiation: 465 nm, 6.5 mW/cm^2, 40 min. Monobromobimane: λ_{ex} =405 nm, λ_{em} = 460–540 nm. C11-BODIPY$^{581/591}$: λ_{ex} =488 nm, λ_{em} = 490–650 nm. (f) The scheme of the mechanism of ferroptosis.

eration ability of the Ir(III) complex, PDT post therapy could induce severe tumor hypoxia, which is favorable for the activation of AQ4N, contributing to the effective cancer treatment outcomes. Meanwhile, ROS damage the liposome and the sorfenib was released for targeting chemotherapy. This AQ4N-**Ir1**-sorafenib-liposome shows several advantages as a multifunctional cancer theranostic: (1) its sequential activation pattern could contribute to a promising synergistic cancer treatment strategy by taking advantage of the PDT-induced tumor hypoxia and activating hypoxic prodrug; (2) its targeting therapy could improve the drug resistance of sorafenib in the treatment of HCC; (3) its excellent biocompatibility and well defined composition would make it a promising candidate for clinical translation in future.

Declaration of competing interest

The authors declared that they have no conflicts of interest to this work. They declare that they do not have any commercial or associative interest that represents a conflict of interest in connection with the work submitted.

Acknowledgments

We appreciate the financial support of the National Natural Science Foundation of China (NSFC, Nos. 22077085, 22007104, 22177078, 21907069), the Project of the Natural Science Foundation of Guangdong Province (No. 2019A1515011958) and the Science and Technology Foundation of Shenzhen (Nos. JCYJ20210324095200002 and JCYJ20190808153209537). We appreciate the Instrumental Analysis Center of Shenzhen University.

Supplementary materials

Supplementary material associated with this article can be found, in the online version, at doi:10.1016/j.cclet.2022.07.009.

References

[1] T. Akinyemiju, S. Abera, M. Ahmed, et al., JAMA Oncol. 3 (2017) 1683–1691.
[2] Y. Sun, L. Wu, Y. Zhong, et al., Cell 184 (2021) 404–421.
[3] A.S. Kekule, U. Lauer, M. Meyer, et al., Nature 343 (1990) 457–461.
[4] R. Rudalska, D. Dauch, T. Longerich, et al., Nat. Med. 20 (2014) 1138–1146.
[5] J.M. Llovet, S. Ricci, V. Mazzaferro, et al., N. Engl. J. Med. 359 (2008) 378–390.
[6] M.M. Gounder, M.R. Mahoney, B.A. Van Tine, et al., N. Engl. J. Med. 379 (2018) 2417–2428.
[7] C. Wang, S. Vegna, H. Jin, et al., Nature 574 (2019) 268–272.
[8] Z. Dong, L. Feng, Y. Hao, et al., J. Am. Chem. Soc. 140 (2018) 2165–2178.
[9] B. Liu, C. Li, Z. Cheng, et al., Biomater. Sci. 4 (2016) 890–909.
[10] F. Liu, Y. Ma, L. Xu, et al., Biomater. Sci. 3 (2015) 1218–1227.
[11] Y.L. Hu, M. DeLay, A. Jahangiri, et al., Cancer Res. 72 (2012) 1773–1783.
[12] D. Ackerman, M.C. Simon, Trends Cell Biol. 24 (2014) 472–478.
[13] R.C. Ji, Cancer Lett. 346 (2014) 6–16.
[14] P. Prasad, C.R. Gordijo, A.Z. Abbasi, et al., ACS Nano 8 (2014) 3202–3212.
[15] J. Dang, H. He, D. Chen, et al., Biomater. Sci. 5 (2017) 1500–1511.
[16] A. Rapisarda, G. Melillo, Nat. Rev. Clin. Oncol. 9 (2012) 378–390.
[17] A. Chowdhury, R. Dasgupta, Appl. Opt. 56 (2017) 439–445.
[18] S. Wang, F. Yuan, K. Chen, et al., Biomacromolecules 16 (2015) 2693–2700.
[19] G. Song, C. Liang, X. Yi, et al., Adv. Mater. 28 (2016) 2716–2723.
[20] X. Song, J. Xu, C. Liang, et al., Nano Lett. 18 (2018) 6360–6368.

[21] R. Zhang, X. Song, C. Liang, et al., Biomaterials 138 (2017) 13–21.
[22] H. Wang, Y. Chao, J. Liu, et al., Biomaterials 181 (2018) 310–317.
[23] X. Song, L. Feng, C. Liang, et al., Nano Res. 10 (2017) 1200–1212.
[24] M.R. Junttila, F.J. de Sauvage, Nature 501 (2013) 346–354.
[25] W.A. Denny, Lancet Oncol. 1 (2000) 25–29.
[26] G.J. Weiss, J.R. Infante, E.G. Chiorean, et al., Clin. Cancer Res. 17 (2011) 2997.
[27] K.J. Williams, M.R. Albertella, B. Fitzpatrick, et al., Mol. Cancer Ther. 8 (2009) 3266.
[28] L. Feng, L. Cheng, Z. Dong, et al., ACS Nano 11 (2017) 927–937.
[29] H. Zhao, B. Zhao, L. Li, et al., Adv. Healthc. Mater. 9 (2020) 1901335.
[30] C. Wu, Q. Liu, Y. Wang, et al., Chin. Chem. Lett. 32 (2021) 2400–2404.
[31] Q. Zhu, X. Ling, Y. Yang, et al., Adv. Sci. 6 (2019) 1801899.
[32] C. Zhang, J. Wu, W. Liu, et al., ACS Appl. Bio Mater. 3 (2020) 3817–3826.
[33] Z. Li, Q. Xu, X. Lin, et al., Chin. Chem. Lett. 33 (2022) 1875–1879.
[34] J. Yan, Y. Zhang, L. Zheng, et al., Chin. Chem. Lett. 33 (2022) 767–772.
[35] J. Zhao, W. Wu, J. Sun, et al., Chem. Soc. Rev. 42 (2013) 5323–5351.
[36] T. Yogo, Y. Urano, Y. Ishitsuka, et al., J. Am. Chem. Soc. 127 (2005) 12162–12163.
[37] S.G. Awuah, J. Polreis, V. Biradar, et al., Org. Lett. 13 (2011) 3884–3887.
[38] J.S. Nam, M.G. Kang, J. Kang, et al., J. Am. Chem. Soc. 138 (2016) 10968–10977.
[39] L. He, M.F. Zhang, Z.Y. Pan, et al., Chem. Commun. 55 (2019) 10472–10475.
[40] J. Li, L. Zeng, K. Xiong, et al., Chem. Commun. 55 (2019) 10972–10975.
[41] S. Monro, K.L. Colón, H. Yin, et al., Chem. Rev. 119 (2019) 797–828.
[42] C.P. Tan, Y.M. Zhong, L.N. Ji, et al., Chem. Sci. 12 (2021) 2357–2367.
[43] C. Imberti, P. Zhang, H. Huang, et al., Angew. Chem. Int. Ed. 59 (2020) 61–73.
[44] X. Wang, X. Wang, S. Jin, et al., Chem. Rev. 119 (2019) 1138–1192.
[45] C. Jin, F. Liang, J. Wang, et al., Angew. Chem. Int. Ed. 59 (2020) 15987–15991.
[46] L. Hao, Z.W. Li, D.-Y. Zhang, et al., Chem. Sci. 10 (2019) 1285–1293.
[47] P. Zhang, C.K.C. Chiu, H. Huang, et al., Angew. Chem. Int. Ed. 56 (2017) 14898–14902.
[48] H. Huang, S. Banerjee, K. Qiu, et al., Nat. Chem. 11 (2019) 1041–1048.
[49] C. Huang, C. Liang, T. Sadhukhan, et al., Angew. Chem. Int. Ed. 60 (2021) 9474–9479.
[50] J. Zhu, A. Ouyang, Z. Shen, et al., Chin. Chem. Lett. 33 (2022) 1907–1912.
[51] K.N. Wang, L.Y. Liu, G. Qi, et al., Adv. Sci. 8 (2021) 2004379.
[52] Z. Fan, Y. Rong, T. Sadhukhan, et al., Angew. Chem. Int. Ed. 61 (2022) e202202098.
[53] Q. Yang, H. Jin, Y. Gao, et al., ACS Appl. Mater. Interfaces 11 (2019) 15417–15425.
[54] S.J. Dixon, K.M. Lemberg, M.R. Lamprecht, et al., Cell 149 (2012) 1060–1072.
[55] W.S. Yang, R. SriRamaratnam, M.E. Welsch, et al., Cell 156 (2014) 317–331.
[56] V.E. Kagan, G. Mao, F. Qu, et al., Nat. Chem. Biol. 13 (2017) 81–90.
[57] D. Qi, L. Xing, L. Shen, et al., Chin. Chem. Lett. 33 (2022) 4595–4599.
[58] X. Meng, J. Deng, F. Liu, et al., Nano Lett. 19 (2019) 7866–7876.
[59] T. Liu, W. Liu, M. Zhang, et al., ACS Nano 12 (2018) 12181–12192.
[60] M.J. Hangauer, V.S. Viswanathan, M.J. Ryan, et al., Nature 551 (2017) 247–250.
[61] L. Feng, M. Gao, D. Tao, et al., Adv. Funct. Mater. 26 (2016) 2207–2217.
[62] C.R. Nishida, P.R. Ortiz de Montellano, J. Med. Chem. 51 (2008) 5118–5120.
[63] S.M. Raleigh, E. Wanogho, M.D. Burke, et al., Int. J. Radiat. Oncol. Biol. Phys. 42 (1998) 763–767.
[64] H. Li, W. Shi, X. Li, et al., J. Am. Chem. Soc. 141 (2019) 18301–18307.
[65] E.M. Kosower, N.S. Kosower, Meth. Enzymol. 251 (1995) 133–148.
[66] G.L. Newton, R.C. Fahey, Meth. Enzymol. 251 (1995) 148–166.
[67] Y. Zou, M.J. Palte, A.A. Deik, et al., Nat. Commun. 10 (2019) 1617.
[68] T. Xu, Y. Ma, Q. Yuan, et al., ACS Nano 14 (2020) 3414–3425.
[69] R. Xu, J. Yang, Y. Qian, et al., Nanoscale Horiz. 6 (2021) 348–356.